Available online at www.sciencedirect.com
ScienceDirect
Acta Materialia 59 (2011) 521–530
Acta MATERIALIA
www.elsevier.com/locate/actamat

# Magnetic phase diagram of the Fe–Ni system

W. Xiong [a,b,*], H. Zhang [c], L. Vitos [c], M. Selleby [a]

[a] Division of Computational Thermodynamics, Department of Materials Science and Engineering, KTH (Royal Institute of Technology), Brinellvägen 23, SE-100 44 Stockholm, Sweden
[b] State Key Lab of Powder Metallurgy, Central South University, Changsha 410083, China
[c] Division of Applied Physics, Department of Materials Science and Engineering, KTH (Royal Institute of Technology), Brinellvägen 23, SE-100 44 Stockholm, Sweden

Received 9 July 2010; received in revised form 16 September 2010; accepted 27 September 2010
Available online 26 October 2010

**Abstract**

Magnetic phase diagrams of body-centered cubic and face-centered cubic Fe–Ni alloys were constructed using available experimental data and ab initio calculations. The results show that significant improvements in the "standard" diagrams (handbooks and CALPHAD databases) are required. The present work demonstrates that the CALPHAD magnetic model is not sophisticated enough to describe the Fe–Ni system. In addition, a new thermodynamic description of the lattice stability for pure Ni is urgently needed, since the recommended magnetic properties for CALPHAD modeling are distinct from the experimental and ab initio results. This work indicates that the construction of magnetic phase diagrams is indispensable during the phase transformation study of magnetic systems.


*Keywords:* Invar alloy; Magnetic properties; Thermodynamics; Steels; Martensitic phase transformation

## 1. Introduction

Because of their anomalous low thermal coefficient, the Invar alloys have attracted many investigations. It is well known that the anomalous physical properties of Invar alloys are closely related to their magnetic properties [1]. In addition, being an important component in steels, there are many studies of the thermodynamics for this binary. Also, investigation of the martensitic transformation in the Fe-rich part could benefit from the present study of the magnetism of Fe–Ni alloys (see Ref. [2] and references therein).

The Fe–Ni phase diagram has been constructed by the CALPHAD (CALculation of PHAse Diagram) community [3–6] and reviewed in the ASM handbooks [7,8]. As far as the present authors know, these have been considered "standard" references in all subsequent studies and also adopted in numerous thermodynamic databases. In spite of extensive thermodynamic investigations, a study on the magnetic phase diagram of the Fe–Ni binary is still lacking. Those constructed in the handbooks [7,8], which focus only on temperatures >500 K, are not acceptable, as will be shown later. In addition, not enough attention has been paid to the metastable phase regions. Therefore, it is interesting to perform an ab initio study on Fe–Ni alloys to complement the reported experiments. The present study will construct the magnetic Fe–Ni phase diagram for the ferromagnetic and paramagnetic states, and also reveal that the magnetic model used in the CALPHAD approach needs to be improved.

## 2. Experimental data

First, a thorough literature survey was performed on the measurement of the magnetic transition temperature ($T_*$) and the mean magnetic moment ($\bar{\beta}$) of the Fe–Ni body-centered cubic (bcc) and face-centered cubic (fcc) alloys for magnetic transition among antiferromagnetic, ferromag-

* Corresponding author at: Division of Computational Thermodynamics, Department of Materials Science and Engineering, KTH (Royal Institute of Technology), Brinellvägen 23, SE-100 44 Stockholm, Sweden. Tel.: +46 8 7908313; fax: +46 8 100411.
*E-mail address:* wxiong@yahoo.com (W. Xiong).

1359-6454/$36.00 
doi:10.1016/j.actamat.2010.09.055

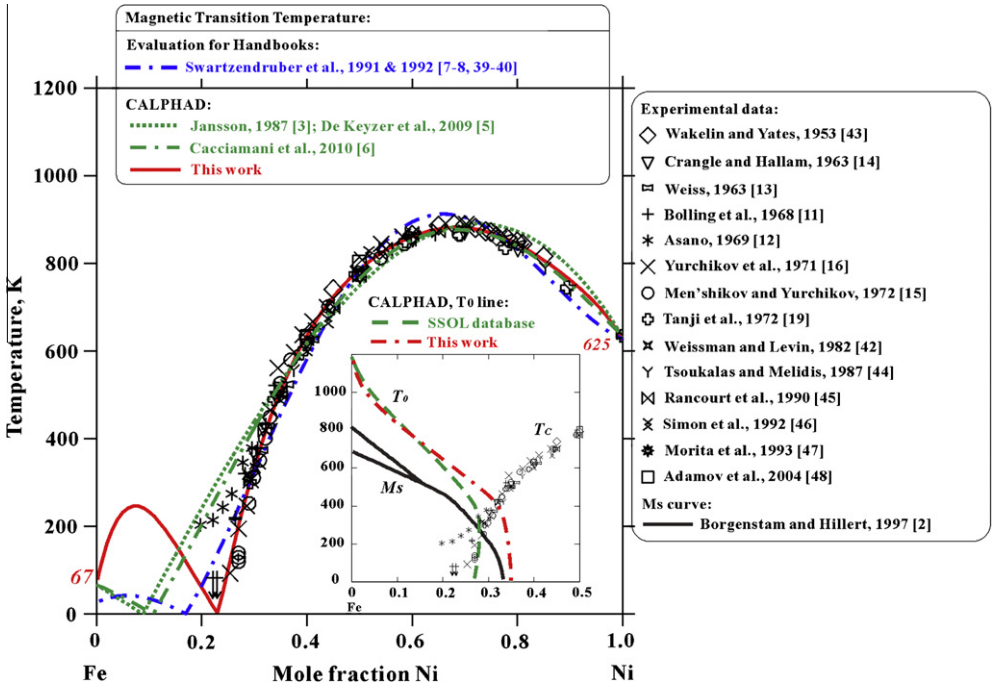


Fig. 1. Comparison between calculated and experimental magnetic transition temperatures of the fcc phase. The small sub-figure at the bottom right shows the evaluated martensitic transformation curve [2] (black solid line) and the model-predicted $T_0$ line according to the SSOL database (green dashed line) [38] and this work (red chained line). The magnetic parameters adopted in the SSOL database are taken from the work by Jansson [3]. (For interpretation of the references to colour in this figure legend, the reader is referred to the web version of this article.)

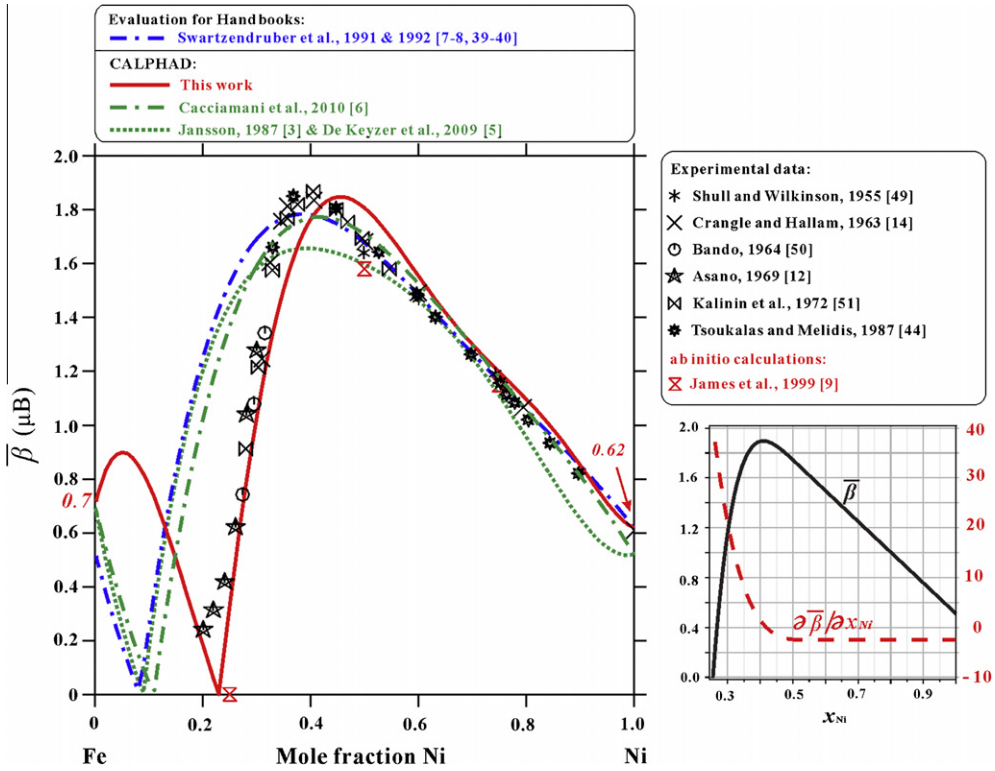


Fig. 2. Comparison of $\bar{\beta}$ of the fcc Fe–Ni alloys at the ferromagnetic state. The small sub-figure on the right-hand side illustrates the variation in $\bar{\beta}$ in the ferromagnetic state with Ni composition. (For interpretation of the references to colour in this figure legend, the reader is referred to the web version of this article.)

netic and paramagnetic states. All the available experimental data are summarized in Figs. 1–4. It is noted that ab initio calculations of $\bar{\beta}$ for the fcc alloys in the ferromagnetic state were performed recently by James et al. [9] using the coherent

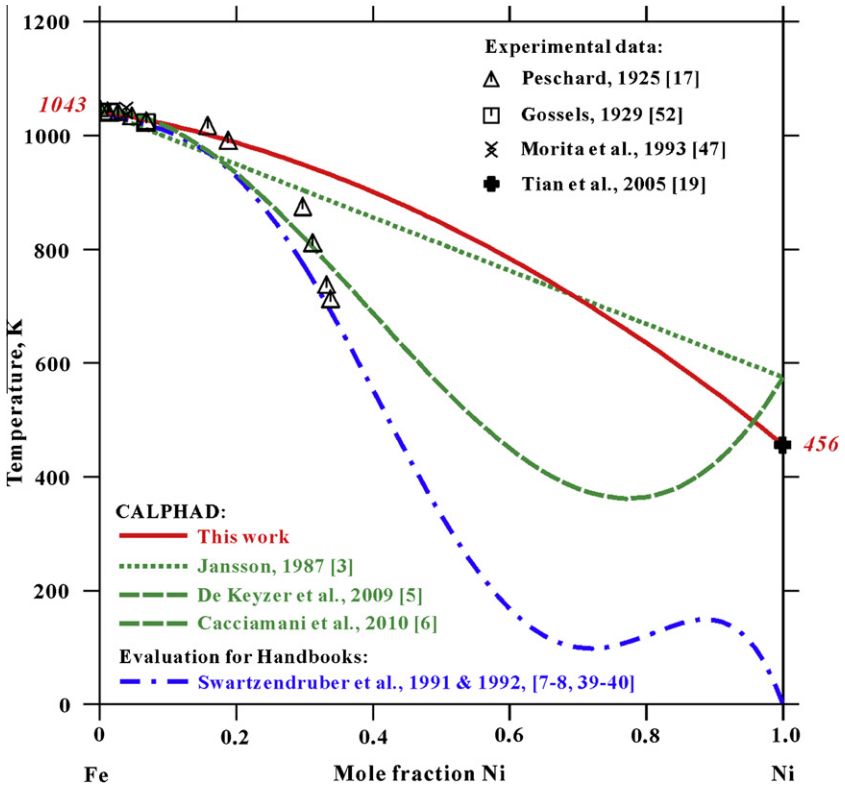


Fig. 3. Curie temperature of the bcc Fe–Ni alloys. Blue chained line corresponds to the evaluation in the handbooks [7,8] according to Refs. [39,40]. (For interpretation of the references to colour in this figure legend, the reader is referred to the web version of this article.)

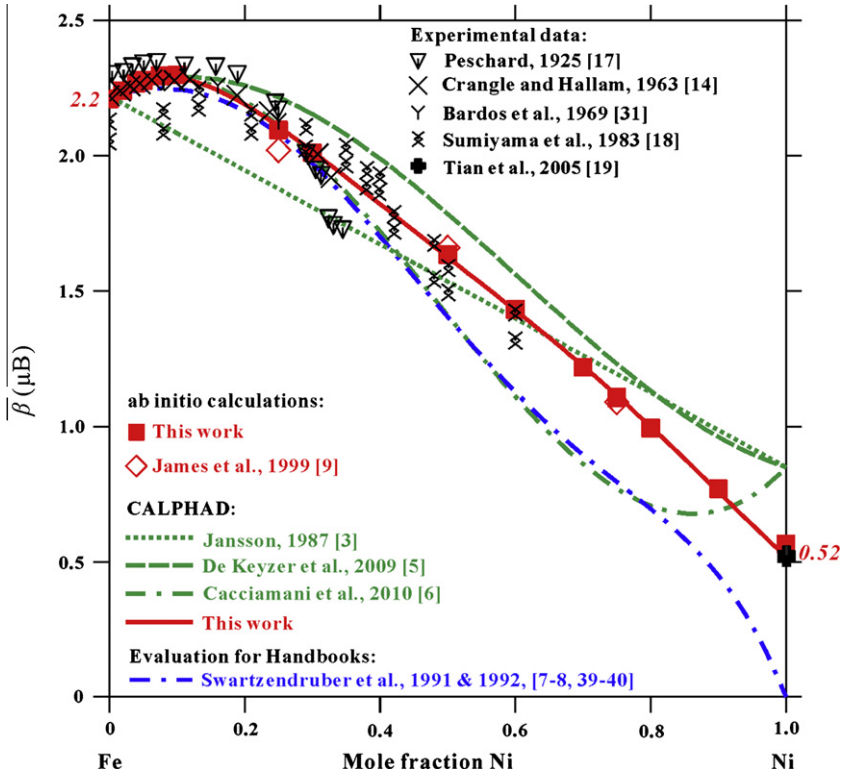


Fig. 4. $\bar{\beta}$ of the bcc Fe–Ni alloys at the ferromagnetic states. Blue chained line stands for the evaluation in the handbooks [7,8] according to Refs. [39,40]. (For interpretation of the references to colour in this figure legend, the reader is referred to the web version of this article.)

potential approximation (CPA) in combination with a linear muffin-tin orbitals basis set.

Apparently, the largest divergence of the experimental $T_C$ (the Curie temperature) of the fcc alloys belongs to those with Ni content <30 at.%. It is true that measurements on the metastable fcc alloys are difficult. In the experiments, the alloys are quenched from high temperatures in the stable fcc region, and later subjected to magnetic determination for $T_C$ and $\bar{\beta}$. As shown in Fig. 1, the alloys with $M_S$ (martensite start temperature) >300 K contain <30 at.% Ni. According to the experiments by Golovchiner [10], during martensitic transformation, the phase transition-induced elastic stresses can lead to an increase in the lattice parameter of the ($\gamma$-fcc) phase because of its coherent bond with the lattice of ferrite. As a consequence, it is quite important to suppress the martensitic transformations in the samples. In the work of Bolling et al. [11], the interstitially dissolved carbon was used to inhibit the martensitic transformation and fortuitously increase the propensity for ferromagnetism. Linear extrapolation to zero carbon was used to achieve $T_C$ and $\bar{\beta}$ as given in Fig. 1. In the work of Asano [12], as another possibility to circumvent the martensitic transformation, finely grained Fe–Ni particles were used because of their lower $M_S$ temperatures compared with bulk alloys, but the antiferromagnetic clusters were formed in the ferromagnetic matrix. Therefore, the magnetic two-phase state was retained up to higher temperatures [12], as shown in Fig. 1, and is obviously inconsistent with the other experimental data [13–16].

In Fig. 2, apart from Ref. [12], it is found that there are no other measurements on $\bar{\beta}$ performed for alloys with Ni content <27 at.%. However, the ab initio calculations by James et al. [9] indicates that the transition from ferromagnetism to antiferromagnetism at the ground state is expected to be at 25 at.% Ni, the same as for $T_*$ discussed above.

In the case of bcc alloys, as shown in Fig. 3, experimentally measured $T_C$ data are scarce. Therefore, it is very hard to make any judgment about the accuracy of the work by Peschard [17]. In contrast, there are more measurements on $\bar{\beta}$, as shown in Fig. 4. Experimental data show a maximum of $\bar{\beta}$ in the vicinity of 9 at.% Ni. It is worth mentioning that the stable bcc phase region is quite limited according to the phase diagram shown in Fig. 5. Therefore, the values of $\bar{\beta}$ are determined mainly from the Ni thin films, which grow on some special substrates [18,19]. For example, in the work of Tian et al. [19], the magnetic moment of bcc Ni was determined from the Ni thin films by epitaxial growth on the GaAs single crystal substrate with {0 0 1} parallel to the surface. Although the experimental $\bar{\beta}$ in Fig. 4 are scattered, it is noticed that the experimental data for alloys with ~35 at.% Ni by Peschard [17] are lower than the rest. In order to make an impartial judgment on the experimental $T_C$ of Peschard [17], ab initio calculations were performed on $\bar{\beta}$ for a series of bcc alloys in the ferromagnetic state. The available ab initio calculations by James et al. [9] for three compositions are considered too limited.

## 3. Ab initio calculations

The present ab initio calculations are based on the density functional theory [20] formulated within the Perdew–Burke–Ernzerhof generalized gradient approximation for the exchange–correlation functional [21]. The Kohn–Sham equations [22] are solved using the exact muffin-tin orbitals (EMTO) method [23–25], and for the total energy calculation the full charge density technique is used [24,26]. The substitutional disorder is treated within the CPA [24,27,28]. The EMTO approach ensures the accuracy needed for the calculation of the anisotropic lattice distortions in random alloys. In the present application, the one-electron equations are solved within the scalar-relativistic and soft core approximations. The Green function is calculated for 16 complex energy points distributed exponentially on a semicircular contour. The EMTO basis set includes $p$, $d$ and $f$ orbitals ($l_{\max} = 3$), and in the one-center expansion of the full charge density, $l^h_{\max} = 8$ is used. All calculations are performed for ferromagnetic bcc alloys. About 2000 uniformly distributed $k$-points are used in the irreducible wedge of the bcc Brillouin zone. The electrostatic correction to the single-site CPA was described using the screened impurity model [29] with a screening parameter of 0.6. For the Fe–Ni alloy considered, the potential sphere radius was chosen to be equal to the corresponding average atomic sphere radius. All calculations were performed for static lattice (neglecting the phonon contributions).

Using the EMTO method, the magnetic moments of the random ferromagnetic bcc $Fe_{1-x}Ni_x$ ($0 \leqslant x \leqslant 1$) were calculated as a function of the chemical composition. At each concentration $x$, the theoretical equilibrium lattice parameter $a(x)$ was derived from an exponential Morse-type function [30] fitted to the ab initio total energies calculated for seven different atomic volumes. Then the magnetic moment of $Fe_{1-x}Ni_x$ was obtained at the corresponding equilibrium lattice constant.

The magnetic moment of alloy component $\alpha$ within the Wigner–Seitz cell is calculated. The spin density of component $\alpha$ on site $Q$ with spin $S$ is $n^{\alpha}_{QS}(\mathbf{r})$, where $\mathbf{r}$ stands for the real space vector. The corresponding magnetic moment density is the difference between the spin density with spin up and the one with spin down, namely, $m^{\alpha}_{QS}(\mathbf{r}) = n^{\alpha}_{Q\uparrow}(\mathbf{r}) - n^{\alpha}_{Q\downarrow}(\mathbf{r})$. The magnetic moment for component $\alpha$ on site $Q$ is obtained by integrating $m^{\alpha}_{QS}(\mathbf{r})$ within the Wigner–Seitz cell, $\bar{\beta}_Q{}^{\alpha} = \int_{\Omega Q} m^{\alpha}_{QS}(\mathbf{r}) d\mathbf{r}$. Then the total magnetic moment of the alloy is defined as the average of magnetic moments of the alloy components, $\bar{\beta}_Q = \sum_{\alpha} c_{\alpha} \cdot \beta^{\alpha}_Q$, where $c$ is the impurity concentration.

The present calculated average magnetic moments are shown in Fig. 4 and listed in Table 1, together with the equilibrium lattice parameters and individual magnetic moments. It is found that the value of $\bar{\beta}$ for $Fe_{1-x}Ni_x$ alloys increases monotonously with Ni concentration up to ~7.5 at.%. Above this limit, $\bar{\beta}$ decreases almost linearly from the maximum of $2.40\mu_B$ at $Fe_{0.925}Ni_{0.075}$ to $0.57\mu_B$ corresponding to pure bcc Ni. The magnetic moment of

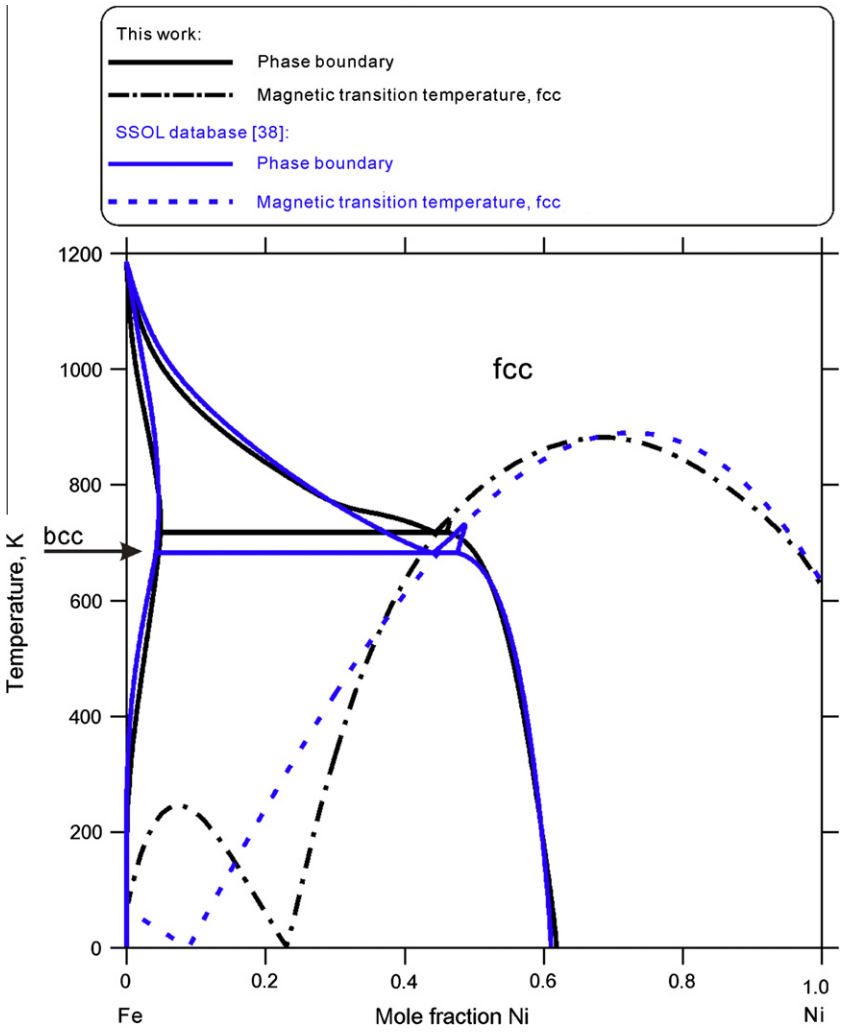


Fig. 5. Comparison of the calculated phase diagram under 1200 K between this work and the SSOL database. (For interpretation of the references to colour in this figure legend, the reader is referred to the web version of this article.)

Table 1
The present ab initio equilibrium lattice parameter, mean magnetic moments and site projected magnetic moments for ferromagnetic bcc Fe–Ni alloys.

| $x$ (Ni) | $a$ (nm) | $\bar{\beta}$ ($\mu_B$) | $\beta_{Fe}$ ($\mu_B$) | $\beta_{Ni}$ ($\mu_B$) |
|---|---|---|---|---|
| 0 | 0.28368 | 2.282 | 2.282 | – |
| 0.02 | 0.28428 | 2.328 | 2.357 | 0.912 |
| 0.04 | 0.28487 | 2.369 | 2.430 | 0.907 |
| 0.05 | 0.28514 | 2.383 | 2.461 | 0.905 |
| 0.075 | 0.28569 | 2.396 | 2.518 | 0.895 |
| 0.10 | 0.28602 | 2.371 | 2.538 | 0.868 |
| 0.25 | 0.28577 | 2.144 | 2.607 | 0.753 |
| 0.30 | 0.28547 | 2.054 | 2.623 | 0.726 |
| 0.50 | 0.28422 | 1.668 | 2.689 | 0.646 |
| 0.60 | 0.28353 | 1.462 | 2.729 | 0.617 |
| 0.70 | 0.28279 | 1.244 | 2.771 | 0.590 |
| 0.75 | 0.28241 | 1.139 | 2.798 | 0.586 |
| 0.80 | 0.28202 | 1.027 | 2.823 | 0.578 |
| 0.90 | 0.28120 | 0.793 | 2.867 | 0.562 |
| 0.99 | 0.28050 | 0.589 | 2.908 | 0.566 |
| 1.00 | 0.28041 | 0.566 | – | 0.566 |

the Fe component is found to increase monotonously with increasing Ni concentration from $2.28\mu_B$ for pure bcc Fe to $2.91\mu_B$ corresponding to $Fe_{0.01}Ni_{0.99}$. Compared with the obvious decreasing behavior of the average magnetic moment of ferromagnetic bcc $Fe_{1-x}Ni_x$ alloys, the individual change in the magnetic moment of Ni is relatively small. The magnetic moment of Ni decreases slightly from the maximum of $0.91\mu_B$ at $Fe_{0.98}Ni_{0.02}$ to $0.62\mu_B$ at $Fe_{0.4}Ni_{0.6}$. The magnetic moment of the Ni component remains almost constant ($\sim 0.58\mu_B$) in the Ni concentration range $0.6 \leqslant x \leqslant 1$.

The present ab initio results confirm the experimental finding by Crangle and Hallam [14], Peschard [17] and Bardos et al. [31], namely that $\bar{\beta}^{bcc}$ reaches a maximum value of $\sim 2.3\mu_B$ at ~9 at.% Ni.

## 4. CALPHAD modeling

### 4.1. Magnetic model

Before comparing the available CALPHAD modeling with experimental and ab initio data, it is necessary briefly to introduce the magnetic model currently used in the

CALPHAD approach. The Gibbs energy of a solution phase $\varphi$, such as fcc and bcc, is expressed as:

$$G_m^{\varphi} = x_{Fe}\cdot {}^{o}G_{Fe}^{\varphi} + x_{Ni}\cdot {}^{o}G_{Ni}^{\varphi} + RT(x_{Fe}\ln x_{Fe} + x_{Ni}\ln x_{Ni}) + {}^{ex}G_m^{\varphi} + {}^{mag}G_m^{\varphi} \quad (1)$$

where ${}^{o}G_{Fe}^{\varphi}$ and ${}^{o}G_{Ni}^{\varphi}$ are the Gibbs energy in the $\varphi$ state of pure Fe or Ni, respectively. The third term in Eq. (1) corresponds to the contribution to Gibbs energy from the ideal entropy of mixing, the fourth term to the excess Gibbs energy, and the last term to the magnetic contribution, given by the following equation:

$${}^{mag}G_m^{\varphi} = RT\cdot\ln\left(\bar{\beta}^{\varphi}+1\right)\cdot g(\tau) \quad (2)$$

where $\tau$ is $T/T_*$, $T_*$ being $T_C$ (the Curie temperature) for ferromagnetic materials or $T_N$ (the Néel temperature) for antiferromagnetic materials. The contributions to the Gibbs energy due to magnetic transitions are thus modeled separately. $T_*$ and $\bar{\beta}$ for different phase are described as functions of composition using the Redlich–Kister polynomial [32], i.e.,

$$T_*^{\varphi} = T_{*,Fe}^{\varphi}\cdot x_{Fe} + T_{*,Ni}^{\varphi}\cdot x_{Ni} + x_{Fe}x_{Ni}\left[a_0 + a_1(x_{Fe}-x_{Ni}) + a_2(x_{Fe}-x_{Ni})^2 + \cdots + a_i(x_{Fe}-x_{Ni})^i\right] \quad (3)$$

$$\bar{\beta}_{\varphi} = \beta_{Fe}^{\varphi}\cdot x_{Fe} + \beta_{Ni}^{\varphi}\cdot x_{Ni} + x_{Fe}x_{Ni}\left[b_0 + b_1(x_{Fe}-x_{Ni}) + b_2(x_{Fe}-x_{Ni})^2 + \cdots + b_i(x_{Fe}-x_{Ni})^i\right] \quad (4)$$

where $T_{*,Fe}^{\varphi}$ and $T_{*,Ni}^{\varphi}$ are the Curie/Néel temperatures for Fe and Ni, respectively. These are normally taken from the SGTE (Scientific Group Thermodata Europe) collection of the element properties [33]. $a$ and $b$ are the constants in the Redlich–Kister polynomial term used to fit experimental $T_*$ and $\bar{\beta}$.

In Eq. (2), $g(\tau)$ is a simplified function depending on structure.

$$g(\tau) = \begin{cases} 1 - \frac{1}{A}\left[\frac{79\cdot\tau^{-1}}{140\cdot p} + \frac{474}{497}\cdot\left(\frac{1}{p}-1\right)\left(\frac{\tau^3}{6}+\frac{\tau^9}{135}+\frac{\tau^{15}}{600}\right)\right]; & \tau < 1 \\ -\frac{1}{A}\left(\frac{\tau^{-5}}{10}+\frac{\tau^{-15}}{315}+\frac{\tau^{-25}}{1500}\right); & \tau \geqslant 1 \end{cases} \quad (5)$$

with

$$A = \frac{518}{1125} + \frac{11692}{15975}\cdot\left(\frac{1}{p}-1\right) \quad (6)$$

in which $p$ is an empirical constant related to structure [34]. It also stands for the ratio of the energy contributions to the magnetic enthalpy below and above the critical temperature $T_*$. In CALPHAD modeling, $p = 0.4$ for bcc crystals, and $p = 0.28$ for fcc and hcp crystals.

It is worth mentioning that, in the CALPHAD model, an antiferromagnetic factor of $-3$ for fcc and $-1$ for bcc is adopted. This treatment can be traced back to Tauer and Weiss [35,36], who found a phenomenological equation between $T_*$ and $\bar{\beta}$ for bcc, fcc and hcp phases of 3d transition alloys. By introducing this type of antiferromagnetic factor (also called the Weiss factor), the Redlich–Kister polynomial can be used as a continuous function spanning the whole composition range to fit $T_*$ and $\bar{\beta}$. However, one should remember that the above magnetic model proposed by Inden [34] and modified by Hillert and Jarl [37] only considers the ferromagnetic, but not antiferromagnetic ordering. Therefore, the empirical Weiss factor is just a numerical treatment without any sound physical meaning.

### 4.2. Available descriptions

In the CALPHAD modeling of a magnetic system, the first step is to perform a comprehensive literature review considering the reported experimental data. Then, the Redlich–Kister polynomial will be employed to describe $T_*$ and $\bar{\beta}$, followed by the optimization of the chemical energy of individual phases.

So far, there are at least four sets of CALPHAD-type parameters for describing $T_*$ and $\bar{\beta}$ of the Fe–Ni system, which are listed in Table 2. The first is reported by Jansson [3] in the thermodynamic description of the Cu–Fe–Ni system. It has been widely used in many commercial thermodynamic databases, e.g., the SSOL database (SGTE Alloy Solutions Database) released by SGTE [38]. Later, a reassessment of the Cu–Fe–Ni system was carried out by Servant et al. [4], but the description of magnetism has not been changed. The second is from the evaluation by Swartzendruber et al. [39,40]. It was later adopted in two important handbooks of phase diagrams, the *ASM Handbook for Phase Diagrams* [8] and *Phase Diagrams of Binary Nickel Alloys* [7]. Recently, a review on the Fe–Ni–Ti system was performed by De Keyzer et al. [5], and the parameters describing the magnetism were modified for the bcc phase of the Fe–Ni system. In Table 2, one can easily find that the description of the Fe–Ni system was modified further after the publication by De Keyzer et al. [5], with another version of parameter sets by Cacciamani et al. [6].

## 5. Discussion

It is discussed in this section that the first parameter set for the Fe–Ni system in the CALPHAD modeling by Jansson [3] cannot reproduce the experimental magnetic phase diagram. Nowadays, it is not clear why such a disagreement between modeling and experiment was accepted. But one possible reason is that the initial assessment of the Fe–Ni system lacked experimental and theoretical information (as mentioned in the book by Lukas et al. [41], p. 94), and it was not corrected in the later CALPHAD modeling, possibly because there was more interest in the high-temperature ranges. But realizing that the problem persists in the most recent publications on Fe–Ni by De Keyzer et al. [5] and Cacciamani et al. [6], the present authors felt that the present work was necessary.

Table 2
The thermodynamic description of $T_*$ and $\bar{\beta}$ for the Fe–Ni system from literature and the present work. There are no thermodynamic parameters used for the bcc phase in Ref. [3].

| Phase | Parameters for $T_*$ and $\bar{\beta}$ | Reference |
|---|---|---|
| fcc | $T_*^{fcc} = -201 \cdot x_{Fe} + 633 \cdot x_{Ni} + x_{Fe}x_{Ni}[2133 - 682(x_{Fe} - x_{Ni})]$ | [3,5] |
| | $\bar{\beta}^{fcc} = -2.1 \cdot x_{Fe} + 0.52 \cdot x_{Ni} + x_{Fe}x_{Ni}\left[9.55 + 7.23(x_{Fe} - x_{Ni}) + 5.93(x_{Fe} - x_{Ni})^2 + 6.18(x_{Fe} - x_{Ni})^3\right]$ | |
| | $T_*^{fcc} = -201 \cdot x_{Fe} + 633 \cdot x_{Ni} + x_{Fe}x_{Ni}[2200 - 700(x_{Fe} - x_{Ni}) - 800(x_{Fe} - x_{Ni})^2]$ | [6] |
| | $\bar{\beta}^{fcc} = -2.1 \cdot x_{Fe} + 0.52 \cdot x_{Ni} + x_{Fe}x_{Ni}[10 + 8(x_{Fe} - x_{Ni}) + 4(x_{Fe} - x_{Ni})^2]$ | |
| | $T_*^{fcc} = -80 \cdot x_{Fe} + 627.4 \cdot x_{Ni} + x_{Fe}x_{Ni}[2040.5 - 1250(x_{Fe} - x_{Ni}) - 2627(x_{Fe} - x_{Ni})^2 - 1784(x_{Fe} - x_{Ni})^3]$ | [39] |
| | $\bar{\beta}^{fcc} = -1.59 \cdot x_{Fe} + 0.62 \cdot x_{Ni} + x_{Fe}x_{Ni}[8.644 + 7.691(x_{Fe} - x_{Ni}) + 4.435(x_{Fe} - x_{Ni})^2 + 0.585(x_{Fe} - x_{Ni})^3]$ | |
| | $T_*^{fcc} = -201 \cdot x_{Fe} + 625 \cdot x_{Ni} + x_{Fe}x_{Ni}[2295.6 - 448.8(x_{Fe} - x_{Ni}) - 1186.0(x_{Fe} - x_{Ni})^2 - 4367.6(x_{Fe} - x_{Ni})^3 - 8658.1(x_{Fe} - x_{Ni})^4 - 5671.0(x_{Fe} - x_{Ni})^5$ | This work |
| | $\bar{\beta}^{fcc} = -2.1 \cdot x_{Fe} + 0.62 \cdot x_{Ni} + x_{Fe}x_{Ni}[10.186 + 8.834(x_{Fe} - x_{Ni}) - 4.006(x_{Fe} - x_{Ni})^2 - 24.828(x_{Fe} - x_{Ni})^3 - 18.686(x_{Fe} - x_{Ni})^4]$ | |
| bcc | $T_*^{bcc} = 1043 \cdot x_{Fe} + 575 \cdot x_{Ni}$ | [3] |
| | $\bar{\beta}^{bcc} = 2.22 \cdot x_{Fe} + 0.85 \cdot x_{Ni}$ | |
| | $T_*^{bcc} = 1043 \cdot x_{Fe} + 575 \cdot x_{Ni} + x_{Fe}x_{Ni}[-1000 - 1500(x_{Fe} - x_{Ni})]$ | [5] |
| | $\bar{\beta}^{bcc} = 2.22 \cdot x_{Fe} + 0.85 \cdot x_{Ni} + x_{Fe}x_{Ni}[1 + 1.6(x_{Fe} - x_{Ni})]$ | |
| | $\bar{\beta}^{bcc} = 2.22 \cdot x_{Fe} + 0.85 \cdot x_{Ni} + x_{Fe}x_{Ni}[-0.5 + 3.5(x_{Fe} - x_{Ni})]$ | [6][a] |
| | $T_*^{bcc} = 1043 \cdot x_{Fe} + x_{Fe}x_{Ni}[-757.6 + 1946(x_{Fe} - x_{Ni}) + 2153(x_{Fe} - x_{Ni})^2 - 2779(x_{Fe} - x_{Ni})^3]$ | [39] |
| | $\bar{\beta}^{bcc} = 2.22 \cdot x_{Fe} + x_{Fe}x_{Ni}[1.176 + 1.445(x_{Fe} - x_{Ni}) + 2.275(x_{Fe} - x_{Ni})^2 - 2.042(x_{Fe} - x_{Ni})^3]$ | |
| | $T_*^{bcc} = 1043 \cdot x_{Fe} + 456 \cdot x_{Ni} + 385.8x_{Fe}x_{Ni}$ | This work |
| | $\bar{\beta}^{bcc} = 2.22 \cdot x_{Fe} + 0.52 \cdot x_{Ni} + x_{Fe}x_{Ni}[1.0177 + 0.5144(x_{Fe} - x_{Ni}) + 1.0733(x_{Fe} - x_{Ni})^2 + 1.0314(x_{Fe} - x_{Ni})^3]$ | |

[a] In Ref. [6], the parameters for describing the Curie temperature of the bcc alloys are the same as in Ref. [5].

### 5.1. Lattice stability of Ni

As shown in Figs. 1–4, none of the above descriptions for Fe–Ni alloys are in agreement with the experimental data [10–18,42–53] or the present ab initio calculations. More seriously, even the lattice stability for Ni in the SGTE compilation [33] needs to be reassessed.

In Table 3, the experimental magnetic transition temperatures and magnetic moment of pure Fe and Ni [14,19,54–59] are compared with the evaluation by SGTE [33] and Swartzendruber et al. [39]. It was found that the recommended value of $T_C$ and $\beta$ for bcc Ni by SGTE [33] needs to be revised as a result of the experiments by Tian et al. [19]. In addition, according to the experiments [14,59], the present value of $\beta$ for fcc Ni seems to be underestimated in the SGTE compilation [33], while the value of $T_C$ is overestimated. In view of the experimental data, the recommended magnetic properties for Fe and Ni are denoted in Figs. 1–4.

Table 3
Comparison of the magnetic properties ($T_C$, $T_N$ and $\beta$) of pure elements, Fe and Ni, between experiments and evaluation.

| Element | Magnetic property | Value and reference | | |
|---|---|---|---|---|
| | | SGTE [33] | Ref. [39] | Experiments |
| Fe | $T_N^{fcc}(K)$ | 67 | 26.6 | 8 [56], 55 [54], 67 [55] |
| | $\beta^{fcc}$ ($\mu_B$) | 0.7 | 0.53 | 0.7 [56], 0.75 [55] |
| | $T_C^{bcc}(K)$ | 1043 | 1043 | 1043 [57] |
| | $\beta^{bcc}$ ($\mu_B$) | 2.22 | 2.22 | 2.22 [58] |
| Ni | $T_C^{fcc}(K)$ | 633 | 627.4 | 625 [59] |
| | $\beta^{fcc}$ ($\mu_B$) | 0.52 | 0.62 | 0.62 [14] |
| | $T_C^{bcc}(K)$ | 575 | 0 | 456 [19] |
| | $\beta^{bcc}$ ($\mu_B$) | 0.85 | 0 | 0.52 [19] |

### 5.2. Comparison of the bcc magnetic phase diagram

As shown in Figs. 3 and 4, in the work of Swartzendruber et al. [39], $T_C$ and $\beta$ of bcc Ni are set to 0, which is obviously unreasonable. Consequently, there is no physical meaning for the parameter used in Ref. [39]. According to the present ab initio calculations, the experimental $\bar{\beta}^{bcc}$ reported by Peschard [17] are much too low compared with the rest of the experimental data [14,18,31]. Therefore, the $T_C$ determined by Peschard [17] also seems lower than the intrinsic temperatures. As shown in Table 2, new sets of parameters have been applied in the work of De Keyzer et al. [5] and Cacciamani et al. [6] to describe the magnetic phase diagram for the bcc phase. However, the modification of the magnetic parameters, which generates minima of the curve for $T_*^{bcc}$ and $\bar{\beta}^{bcc}$, is not supported by any experimental data, as shown in Figs. 3 and 4. In the present work, a set of parameters has been optimized to describe the magnetic properties of Fe–Ni alloys. Because reliable data for $T_C$ of bcc Fe–Ni alloys >10 at.% Ni are lacking, there is no strong change in curvature for the $T_C$ curve assessed in Fig. 3. However, the maximum of $\bar{\beta}^{bcc}$ was reproduced in the present parameter set. It should be mentioned that the experimental data for $T_C^{bcc}$ and $\bar{\beta}^{bcc}$ of Tian et al. [19], rather than the SGTE compilation [33], are adopted to generate the CALPHAD-type parameters in this work.

### 5.3. Comparison of the fcc magnetic phase diagram

In the case of fcc, as discussed above, according to Fig. 1 the precise composition for the kink of the Curie temperature curve at 0 K is difficult to determine. However, according to the ab initio calculations by James et al. [9] given in Fig. 2, the magnetic state will have a transition between

ferromagnetism and antiferromagnetism at 25 at.% Ni, which is reasonable in consideration of the experimental $T_C$ and $\bar{\beta}$. Although great efforts were made to fit the experimental $T_*$ and $\bar{\beta}$ for the fcc phase, there is no chance of achieving a reasonable description within the frame of the present CALPHAD magnetic model. As illustrated in the bottom right-hand sub-figure in Fig. 2, the slope of the $\bar{\beta}^{fcc}$ curve dramatically decreases with decreasing Ni content starting from 45 at.% Ni. The description of the sharp slope change in the $T_*$ and $\bar{\beta}$ curves is absolutely beyond the capability of the Redlich–Kister polynomial. In this work, a temporary parameter set is optimized in Table 2 to describe the magnetic properties of the fcc phase in the form of Redlich–Kister polynomial. However, as shown in Fig. 1, if a good fit of $T_C^{fcc}$ is obtained with a kink at 23 at.% Ni, the Redlich–Kister polynomial will show an arched curve in the antiferromagnetic region. To the best of the authors' knowledge, there is no convincing measured $T_N$ for Fe–Ni alloys. In addition, as mentioned in the previous section, the present CALPHAD magnetic model could not reasonably describe the antiferromagnetic ordering. Therefore, it is better to fit the experimental data in the ferromagnetic region by sacrificing the description of antiferromagnetic region.

In addition, it is difficult to adjust the position of the kink higher than 23 at.% Ni during optimization, and at the same time keep the smooth shape of the $T_*^{fcc}$ curve and a maximum $T_N^{fcc}$ lower than room temperature. More seriously, it is found that a perfect fit to the experimental $\bar{\beta}^{fcc}$ is impossible even for the composition region from 23 to 100 at.% Ni, keeping in mind that the change in magnetic states at ground state requires that the kinks of the curves for $T_*$ and $\bar{\beta}$ should be located at the same composition. Within the frame of the CALPHAD magnetic model, the best fit to $\bar{\beta}^{fcc}$ is shown as a red solid curve in Fig. 2. It is apparent that this curve is not smooth at all >60 at.% Ni. It should be noted that the problems during the fitting to $T_*^{fcc}$ and $\bar{\beta}^{fcc}$ originate from the Redlich–Kister polynomial itself, and it is understandable that the numerous $a$ and $b$ parameters in Eqs. (3) and (4) will cause the calculated curve to fluctuate.

Although the Redlich–Kister polynomial has already been widely used in applied thermodynamics owing to its successful description of the excess properties, such as the Gibbs energy, it is now proved that this type of polynomial is not suitable to describe the magnetic properties of the Fe–Ni system. In fact, the reason for using the Redlich–Kister polynomial to describe $T_*$ and $\bar{\beta}$ in the CALPHAD model is to make all the equations of magnetic properties optimize in a uniform way as the excess Gibbs energy. This also facilitates the description of multi-component cases. Nevertheless, finding some other mathematical form to describe $T_*$ and $\bar{\beta}$ is not easy, owing to the dramatic variation in the curvature of the Fe–Ni system.

Despite the weakness of the CALPHAD magnetic model, the present authors are aware that magnetic phase diagrams were not well studied in many thermodynamic models of magnetic systems. For instance, as pointed out recently in work by Xiong et al. [60], the magnetic phase diagrams of the Fe–Cr system were found to be incorrectly described. However, such an incorrect description has been widely used to establish many multi-component databases.

### 5.4. Prediction of the $T_0$ line

It is now interesting to investigate the consequence of the revised description of the magnetic phase diagrams. In Fig. 1, $T_0$, the temperature at which fcc and bcc of the sample composition would have the same Gibbs energy, is calculated using the SSOL database [38]. The curves of $T_0$ and $M_S$ temperature will cross each other, which is apparently unacceptable, because this means that the martensitic transformation in the alloys with Ni content higher than the crossing point does not require any driving force. In addition, the $T_0$ line will not decrease monotonically. It is known that $T_0$ is difficult to measure, but can only be determined based on the thermodynamic description of the system.

In this work, a set of CALPHAD-type parameters have been assessed for the bcc and fcc phases incorporating the modified magnetic parameters. The low-temperature phase diagram was assessed to be the same as that calculated from the SSOL database [38], which is shown in Fig. 5. The thermodynamic parameters describing the bcc and fcc phases are listed in Table 4, and the parameters to describe $T_*$ and $\bar{\beta}$ can be obtained from Table 2. Owing to the modification of the magnetic transition temperature of the fcc phase, the Nishizawa horn will also change accordingly. However, measurements on the reaction temperature of the monoeutectoid reaction fcc(PM) ↔ fcc(FM) + bcc(FM) (PM, paramagnetic; FM, ferromagnetic) are scarce. Surprisingly, as a consequence of changing the description of the magnetic phase diagram, in Fig. 1, the model-predicted $T_0$ line has a significant shift to the Ni side without crossing the $M_S$ temperature curve, and the $T_0$ line will decrease monotonically along the Ni content. Apparently, such an improvement is due to better description of the magnetic phase diagrams. One can conclude that the reasonable prediction of the $T_0$ line requires a good description not only of phase equilibria, but also of magnetic phase diagrams.

Furthermore, it should be kept in mind that the thermodynamic model of lattice stability validated down to 0 K will

Table 4
Thermodynamic parameters of bcc and fcc phases for the low-temperature phase equilibria in this work[a].

| | |
|---|---|
| *Phase: bcc, Model (Fe, Ni)* | |
| ${}^0L^{bcc}_{Fe,Ni} = -5206.51 + 12.3255 \cdot T$ | ${}^1L^{bcc}_{Fe,Ni} = 10225.35 - 17.7901 \cdot T$ |
| *Phase: fcc, model (Fe, Ni)* | |
| ${}^0L^{fcc}_{Fe,Ni} = -9348.94 + 0.3899 \cdot T$ | ${}^1L^{fcc}_{Fe,Ni} = -21135.90 - 18.5598 \cdot T$ |

[a] In J/mol atom, temperature in Kelvin. The Gibbs energy for the pure elements are from the SGTE compilation [33]. Parameters for the description of magnetic properties can be found in Table 2.

be advantageous in the study of martensitic transformations once the magnetic phase diagram is constructed correctly. It is noteworthy that such an attempt has been made for pure Fe in a recent work by Chen and Sundman [61].

## 6. Concluding remarks

1. Using the EMTO method, $\bar{\beta}$ of a series of bcc alloys were calculated, confirming a maximum in the vicinity of 9 at.% Ni. In addition, the present ab initio calculations confirmed the recent experimental value of $0.52 \pm 0.08\mu_B$ for the magnetic moment of pure bcc Ni in the ferromagnetic state [19].
2. According to this work, the lattice stability for pure Ni in the SGTE compilation, which is now commonly accepted by the CALPHAD community, needs to be modified.
3. The magnetic Fe–Ni phase diagrams for fcc and bcc phases were incorrectly constructed in previous CALPHAD modeling and ASM handbooks. The experimental data show that the transition between antiferromagnetism and ferromagnetism of the fcc phase will be at 25 at.% Ni.
4. It is demonstrated that the description of the magnetic fcc phase diagram of Fe–Ni is beyond the capability of the Redlich–Kister polynomial. Through this work, one could envisage that an improved magnetic model is urgently needed in order to extend the thermodynamic description into low temperature ranges and fill up the gap between CALPHAD and ab initio calculations.
5. The influence of the description on magnetic contribution to Gibbs energy has been demonstrated by prediction of the $T_0$ line, which is the essential information for studying martensitic transformation, but difficult to measure.

## Acknowledgments

This work was performed within the VINN Excellence Hero-m Center, financed by VINNOVA, the Swedish Government Agency of Innovation Systems, Swedish Industry and the Royal Institute of Technology. W.X. is grateful to Drs. A.V. Ruban, and P.A. Korzhavyi, Q. Chen and Prof. M. Hillert for stimulating discussions.

## References

[1] van Schilfgaarde M, Abrikosov IA, Johansson B. Nature (London, UK) 1999;400:46.
[2] Borgenstam A, Hillert M. Acta Mater 1997;45:2079.
[3] Jansson Å. TRITA-MAC-0340, KTH; 1987.
[4] Servant C, Sundman B, Lyon O. CALPHAD 2001;25:79.
[5] De Keyzer J, Cacciamani G, Dupin N, Wollants P. CALPHAD 2009;33:109.
[6] Cacciamani G, Dinsdale A, Palumbo M, Pasturel A. Intermetallics 2010;18:1148.
[7] Swartzendruber LJ, Itkin VP, Alcock CB. Fe–Ni. Phase diagrams of binary nickel alloys. Metals Park (OH): ASM International; 1991. p. 110.
[8] Swartzendruber LJ, Itkin VP, Alcock CB. Fe–Ni. In: Baker H, editor. ASM handbook: alloy phase diagrams, vol. 3. Metals Park (OH): ASM International; 1992.
[9] James P, Eriksson O, Johansson B, Abrikosov IA. Phys Rev B: Condens Matter 1999;59:419.
[10] Golovchiner KY. Phys Met Metallogr 1975;40:175.
[11] Bolling GF, Arrott A, Richman RH. Phys Status Solidi 1968;26:743.
[12] Asano H. J Phys Soc Jpn 1969;27:542.
[13] Weiss RJ. Proc Phys Soc 1963;82:281.
[14] Crangle J, Hallam GC. Proc R Soc Lond, A 1963;272:119.
[15] Men'shikov AZ, Yurchikov EE. Izvestiya Akademii Nauk SSSR. Seriya Fizicheskaya 1972;36:1463.
[16] Yurchikov EE, Menshikov AZ, Tzurin VA. In: Proceedings of the conference on the application of the Mossbauer effect, 17–21 June 1969. Budapest: Akandamiai Kiado; 1971. p. 405.
[17] Peschard M. Revue de Metallurgie 1925;22:663.
[18] Sumiyama K, Kadono M, Nakamura Y. Trans Jpn Inst Met 1983;24:190.
[19] Tian CS, Qian D, Wu D, He RH, Wu YZ, Tang WX, et al. Phys Rev Lett 2005;94:137210.
[20] Hohenberg P, Kohn W. Phys Rev 1964;136:B864.
[21] Perdew JP, Burke K, Ernzerhof M. Phys Rev Lett 1996;77:3865.
[22] Kohn W, Sham LJ. Phys Rev 1965;140:A1133.
[23] Kumar V, Anderson OK, Mookerjee A. Proceedings of the miniworkshop on "Methods of Electronic Structure Calculations" and work. Singapore: World Scientific; 1994.
[24] Vitos L. Phys Rev B 2001;64:014107.
[25] The VitosL, TO EM. Method and applications. London: Springer Verlag; 2007.
[26] Dreysse H. Electronic structure and physical properties of solids: the uses of the LMTO method. Berlin: Springer Verlag; 2000.
[27] Soven P. Phys Rev 1967;156:809.
[28] Gyorffy BL. Phys Rev B 1972;5:2382.
[29] Korzhavyi PA, Ruban AV, Abrikosov IA, Skriver HL. Phys Rev B 1995;51:5773.
[30] Moruzzi VL, Janak JF, Schwarz K. Phys Rev B 1988;37:790.
[31] Bardos DI, Beeby JL, Aldred AT. Phys Rev 1969;177:878.
[32] Redlich O, Kister AT. Ind Eng Chem 1948;40:345.
[33] Dinsdale AT. CALPHAD 1991;15:317.
[34] Inden G. In: Proc CALPHAD, V. Max Planck Institut fuer Eisenforschung, Duesseldorf; 1976. p. 1.
[35] Tauer KJ, Weiss RJ. Phys Rev 1955;100:1223.
[36] Weiss RJ, Tauer KJ. Theory of alloy phases. Cleveland (OH): ASM; 1956. p. 290.
[37] Hillert M, Jarl M. CALPHAD 1978;2:227.
[38] The SGTE general alloys solutions database, SSOL. Version 4.9f. Stockholm: Thermo-Calc AB; 2008.
[39] Swartzendruber L, Itkin V, Alcock C. J Phase Equilib 1991;12:288.
[40] Swartzendruber L, Itkin V, Alcock C. J Phase Equilib 1992;13:585.
[41] Lukas H, Fries SG, Sundman B. Computational thermodynamics: the CALPHAD method. Cambridge: Cambridge University Press; 2007.
[42] Weissman J, Levin L. J Magn Magn Mater 1982;27:347.
[43] Wakelin RJ, Yates EL. Proc Phys Soc, Sect B 1953;66:221.
[44] Tsoukalas Locannis A, Melidis K. Z Metallkd 1987;78:498.
[45] Rancourt DG, Hargraves P, Lamarche G, Dunlap RA. J Magn Magn Mater 1990;87:71.
[46] Simon JP, Lyon O, Faudot F, Boulanger L, Dimitrov O. Acta Metall Mater 1992;40:2693.
[47] Morita H, Fujimori H, Hashimoto S, Wang Z. J Magn Magn Mater 1993;126:173.
[48] Adamov GV, Bukhanov VM, Colligon JS, Minnebaev KF, Nasretdinov AA, Shelyakin LB, et al. In: 16th Ion–surface interactions conference, August 2003, vol. 73. Zvenigorod: Elsevier; 2004. p. 47.
[49] Shull CG, Wilkinson MK. Phys Rev 1955;97:304.
[50] Bando Y. J Phys Soc Jpn 1964;19:237.
[51] Kalinin VM, Kornyakov VA, Khomenko OA, Dunaev FN, Yurchikov EE. Izvestiya Akademii Nauk SSSR. Seriya Fizicheskaya 1972;36:1602.

[52] Gossels G. Z Anorg Allg Chem 1929;182:19.
[53] Tanji Y, Asano H, Moriya H. J Jpn Inst Met 1972;36:1100.
[54] Gonser U, Meechan CJ, Muir AH, Wiedersich H. J Appl Phys 1963;34:2373.
[55] Johanson GJ, McGirr MB, Wheeler DA. Phys Rev B 1970;1:3208.
[56] Abrahams SC, Guttman L, Kasper JS. Phys Rev 1962;127:2052.
[57] Desai PD. J Phys Chem Ref Data 1986;15:967.
[58] Shull CG. Atomic magnetic moments of transition elements in solid solution alloys. Cleveland, OH: American Society for Metals; 1956. p. 279.
[59] Desai PD. Int J Thermophys 1987;8:763.
[60] Xiong W, Selleby M, Chen Q, Odqvist J, Du Y. Crit Rev Solid State Mater Sci 2010;35:125.
[61] Chen Q, Sundman B. J Phase Equilib 2001;22:631.